

Molecular ordering in lipid monolayers: an atomistic simulation

S. Panzuela,^{1,*} D. P. Tieleman,^{2,†} L. Mederos*,^{3,‡} and E. Velasco^{4,§}

¹*Departamento de Física Teórica de la Materia Condensada,
Universidad Autónoma de Madrid, E-28049, Madrid, Spain*

²*Centre for Molecular Simulation and Department of Biological Sciences,
University of Calgary, Calgary, Alberta, Canada*

³*Instituto de Ciencia de Materiales de Madrid,
Consejo Superior de Investigaciones Científicas,*

C/Sor Juana Inés de la Cruz, 3, E-28049, Madrid, Spain

⁴*Departamento de Física Teórica de la Materia Condensada,
Instituto de Ciencias de Materiales Nicolás Cabrera, and IFIMAC,
Universidad Autónoma de Madrid, E-28049, Madrid, Spain*

(Dated: March 18, 2019)

Abstract

We report on atomistic simulations of DPPC lipid monolayers using the CHARMM36 lipid force field and four-point OPC water model. The entire two-phase region where domains of the ‘liquid-condensed’ (LC) phase coexist with domains of the ‘liquid-expanded’ (LE) phase has been explored. The simulations are long enough that the complete phase-transition stage, with two domains coexisting in the monolayer, is reached in all cases. Also, system sizes used are larger than in previous works. As expected, domains of the minority phase are elongated, emphasizing the importance of anisotropic van der Waals and/or electrostatic dipolar interactions in the monolayer plane. The molecular structure is quantified in terms of distribution functions for the hydrocarbon chains and the PN dipoles. In contrast to previous work, where average distributions are calculated, distributions are here extracted for each of the coexisting phases by first identifying lipid molecules that belong to either LC or LE regions. The three-dimensional distributions show that the average tilt angle of the chains with respect to the normal outward direction is $(39.0 \pm 0.1)^\circ$ in the LC phase. In the case of the PN dipoles the distributions indicate a tilt angle of $(110.8 \pm 0.5)^\circ$ in the LC phase and $(112.5 \pm 0.5)^\circ$ in the LE phase. These results are quantitatively different from previous works, which indicated a smaller normal component of the PN dipole. Also, the distributions of the monolayer-projected chains and PN dipoles have been calculated. Chain distributions peak along a particular direction in the LC domains, while they are uniform in the LE phase. Long-range ordering associated with the projected PN dipoles is absent in both phases. These results strongly suggest that LC domains do not exhibit dipolar ordering in the plane of the monolayer, the effect of these components being averaged out at short distances. Therefore, the only relevant component of the molecular dipoles, as regards both intra- and long-range interdomain interactions, is normal to the monolayer. Also, the local orientation of chain projections is almost constant in LC domains and points in the direction along which domains are elongated, suggesting that the line tension driving the phase transition is anisotropic with respect to the interfacial domain boundary. Both van der Waals interactions and interactions from normal dipolar components seem to contribute to an anisotropic line tension, with dipolar in-plane components playing a negligible role.

I. INTRODUCTION

Langmuir monolayers of DPPC in the air-water interface have long been considered a fruitful model system to understand basic physical properties of lung surfactant¹⁻³. A huge body of experimental work has been accumulated over the last decades on this system, focusing on the thermodynamics (surface pressure isotherms), molecular structure, and domain shape and structure⁴⁻⁶. One of the puzzling questions about DPPC monolayers is the possibly nonequilibrium phenomena involved in the growth of domains in the two-phase coexistence region between the liquid-condensed (LC) and liquid-expanded (LE) phases. The difficulty to observe a truly horizontal sector in surface-pressure–area isotherms⁷, together with the observation of persistent, seemingly equilibrated domains with uniform size throughout the coexistence region, may indicate the presence of very long relaxation processes and long-range domain interactions⁸⁻¹¹. Also, some theoretical models have been developed to explain domain shapes and transitions between different shape régimes. These models contain effects from different types of interactions: line tension, curvature, and dipolar components in directions normal and perpendicular to the monolayer. Competition between these interactions leads to interesting shape behaviour, in some cases close to experimental observations of domains in monolayers of pure DPPC molecules. Detailed experimental work^{12,13} and computer simulations^{14-17,23} also exist which suggest models for molecular arrangement of lipid molecules in the monolayers, a question which is also open to debate. The very nature of the relevant interactions is uncertain. A broad consensus exists on the PN dipole orientation, which most studies interpret to be more or less parallel to the monolayer²³⁻²⁵. Also, it has been postulated that the PN dipole is located at slightly different depths in the liquid subphase: as the film is compressed, molecules condense into LC regions and the entire lipid molecules are displaced towards the air phase, thereby expelling solvating water molecules and making the PN region more dehydrated²⁵. These analyses suggest a model where LC domains made of molecules with tightly-packed, tilted (with respect to the monolayer normal) aliphatic chains and strongly interacting dipoles parallel to the monolayer coexist with LE regions with disordered chains and screened parallel dipoles. This view somehow contradicts the assumptions made by many theoretical models for domain shape and shape transitions, based on distributions of strongly interacting dipoles *normal* to the monolayer, with van der Waals (vdW) interactions effectively showing up in

a line-tension contribution which is *isotropic* with respect to the in-plane normal direction at the domain line boundary. The competition between an isotropic line tension and a long-range electrostatic contribution coming from dipoles along the monolayer normal leads to interesting behaviours. In-plane dipolar components have also been contemplated and seen to renormalise the line tension by making it anisotropic²⁶. However, the question is whether assumptions behind these theoretical models are completely correct.

The present work is an attempt to shed some light on some of these issues from the point of view of atomistic simulation, using state-of-the-art force field modelling for both lipid and water molecules, and constitutes a quantitative leap forward with respect to previous simulations in terms of system size and simulation time^{14–17,27–29}. Recently, Javanainen et al.¹⁷ reported on full-atom simulations of DPPC monolayers. Lipid interactions were modelled using the CHARMM36 force field¹⁸, whereas for water molecules the four-point OPC4 force field¹⁹ was used. It was shown that the combination of these two force fields provides quantitative agreement with experimental results on surface pressure isotherms of DPPC monolayers, making this model a suitable tool to also explore structural molecular behaviour. Here we use a simulation setup similar to that of Javanainen et al. to examine in detail the structure of the monolayer in conditions of full phase-separation, where single LC or LE domains coexist with the opposite phase. A novel feature of our analysis is that various molecular distribution functions are identified separately for the two phases, allowing for more accurate measurements of molecular arrangements and orientation. Also, correlation functions describing molecular ordering in both phases are presented. These functions exhibit features corresponding to sustained long-range order of the tails in the LC domains, but PN dipolar heads show almost perfect disorder in azimuthal angles, which indicates that the role of in-plane dipolar components is negligible in determining domain shape and long-range domain interactions.

II. SIMULATIONS

In the present paper we use the same combination of force fields used by Javanainen et al., but on larger system sizes. We run NVT Molecular Dynamics (MD) simulations on systems consisting of 1152 DPPC molecules, distributed in two monolayers (576 molecules per monolayer) and a liquid slab consisting of 93312 water molecules, creating two equiv-

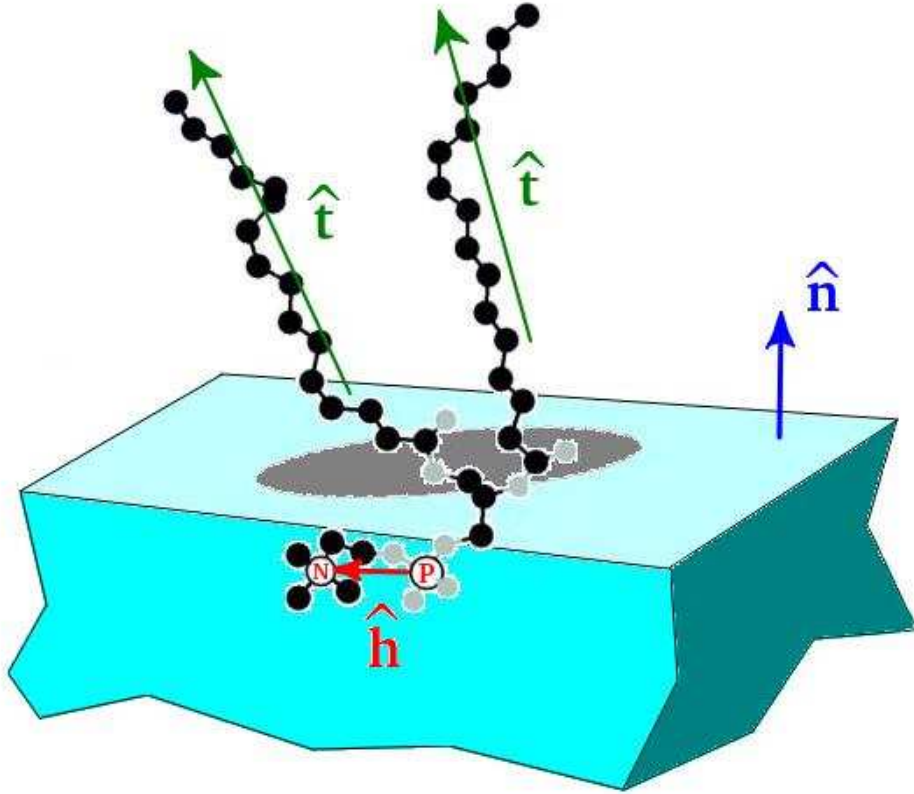


FIG. 1: Schematic of a DPPC molecule showing the definition of the three unit vectors used to describe the orientation of different molecular groups. Also shown is the projection of the molecule on the monolayer plane (see text for details).

alent liquid-vapour interfaces. All systems were built using CHARMM-GUI, a web-based graphical interface that helps create molecular input files for CHARMM-based atomistic simulations. MD simulations were run using the GROMACS 2018.3^{20,21} software on a set of 288 CPU cores for about 21 days of CPU time. Each run spanned a total of 300 ns (simulation time), comprising 50 ns for equilibration and 250 ns for averaging. The systems were thermostatted at 298 K using the Nosé-Hoover technique with coupling parameter 1.0 ps, and a leap-frog algorithm with timestep 0.002 ps was used to integrate the equations of motion.

Fig. 1 is a schematic of a DPPC molecule and its projection on the monolayer plane, showing the definition of the three unit vectors used to describe the orientation of different molecular groups (\hat{h} for the head and \hat{t} for the chains; their precise definitions are given

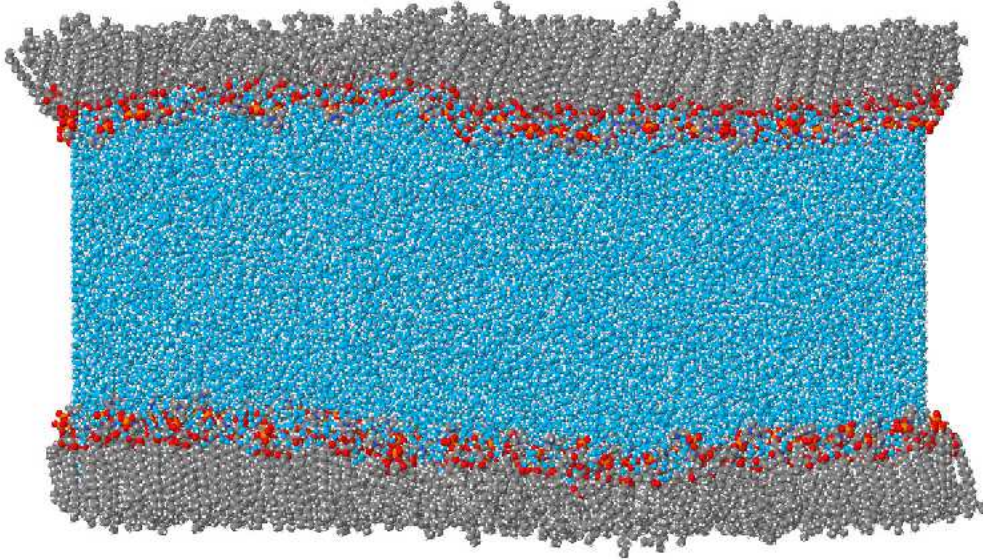


FIG. 2: Edge-on view of molecular configuration of a water liquid slab containing two lipid monolayers with an area per lipid of 65 \AA^2 . Except for small-amplitude interfacial fluctuations, the liquid slab is parallel to the xy plane. The presence of large LC domains at both interfaces is clearly visible.

below). Fig. 2 depicts a molecular configuration of the water slab and lipid molecules adsorbed at the two interfaces, corresponding to two equivalent lipid monolayers. During the course of the simulations no water molecules were detected in the vapour side, which is therefore a vacuum. The monolayers are parallel to the xy plane and perpendicular to the z axis, except for small-amplitude interfacial fluctuations. The simulation box is square in the xy plane with total area $A = L_x L_y$ adjusted to fit the desired two-dimensional inverse density, here expressed, as is customary, as area per lipid in units of \AA^2 . The box length in the z direction, L_z , was set to 22 nm. The number of water molecules used was 93312, giving a thickness of 15 nm. Selected runs were conducted with $L_z = 65$ nm in order to check for possible size effects. Also simulations of a single monolayer were performed to reveal possible effects coming from the interaction between the monolayers mediated by the water slab. In no case was any significant deviation detected, so that all results presented below were obtained with the parameters mentioned above.

Electrostatic interactions were handled with the Particle Mesh Ewald (PME) method²², treating interactions explicitly up to 1.2 nm and using Fast Fourier Transform for the

long-ranged part. All vdW interactions were truncated and shifted at $r_c = 1.2$ nm and corrections to pressure and energy were correspondingly applied. Each run was conducted at constant lateral area and volume to explore different state points along the coexistence line of the LC-LE phase transition. Therefore different mean areas per lipid, from 52 to 76 Å², were analysed which bracket the coexistence density interval. We later report on improved estimates for coexistence densities based on actual measurements of local densities inside domains.

As mentioned in the introduction, the main focus of our work is on domain structure at LC-LE coexistence. Therefore, a reliable method to distinguish lipid molecules in LC domains from lipid molecules in LE domains is required. Since the phase transition involves structural changes that mostly occur in the plane of the monolayer, we need to define a two-dimensional position associated to each lipid molecule. This was done by calculating the centre of mass, projected on the xy plane, of the C=O units of the glycerol group. In this way we associated a two-dimensional position vector $\mathbf{R} = (X, Y)$ to each lipid molecule.

The structural differences between LE and LC regions in the monolayer (see Fig. 3, which is explained in great detail below, for an illustration of the two regions), are well known⁴. In a LE region gauche defects of the two aliphatic chains of a lipid are excited, resulting in disordered chains which interact weakly. Lipids do not show any type of lateral order. By contrast, lipids in a LC domain exhibit straight chains that interact strongly and present a tilted orientation to optimise vdW interactions. As a result, lipid molecules arrange into a stretched local triangular lattice in the plane of the monolayer exhibiting quasi-long range order. The stretching direction coincides with one of the three equivalent axes of the triangular lattice. Different methods have been implemented to distinguish these two types of situations. A popular one is that employed by Baoukina et al.^{6,30}, where a Voronoi network is computed and neighbour numbers are associated to each molecule. In our case we found it more convenient to define a crystalline order parameter $q^{(j)}$ on each lipid molecule, a method borrowed from analyses of two-dimensional crystals. The order parameter at the j th molecule is defined, for each configuration, as

$$q^{(j)} = \left| \sum_{kl} e^{i\mathbf{K}_k \cdot (\mathbf{R}_l - \mathbf{R}_j)} \right|, \quad (1)$$

where $|\dots|$ denotes the modulus of a complex number. The sums run over all positions $\mathbf{R}_l = (X_l, Y_l)$ of the nearest neighbours of the j th molecule, and the reciprocal vectors of

the triangular lattice \mathbf{K}_k . Our simulations show that the direction along which the lattice is stretched coincides with the projected molecular tilt. Moreover, this crystallographic axis is slightly distorted inside the domain. We start by first obtaining the local orientation of the lattice. This is easy if we calculate the unit vector $\hat{\mathbf{t}}$ along each lipid chain (two per DPPC lipid) from the gyration tensor of the chain units (using only the carbon atoms). Next we calculate the order tensor at the j th molecule, $Q^{(j)}$, the components of which are given by

$$Q_{\alpha\beta}^{(j)} = \frac{1}{2} \sum_l \left(3\hat{t}_\alpha^{(l)}\hat{t}_\beta^{(l)} - \delta_{\alpha\beta} \right), \quad \alpha, \beta = 1, 2, 3 \quad (2)$$

where the sum runs over all the neighbours located at a lateral distance within a circle of radius 1.2 nm. The local lattice orientation is now obtained by calculating the eigenvector $\hat{\mathbf{e}}$ associated to the largest eigenvalue of the Q tensor, and then projecting it on the xy monolayer plane. We define the corresponding normalised vector as $\hat{\mathbf{e}}_\perp$. The order parameter $q^{(j)}$ for a given lipid is in the interval $[0, 1]$, with 0 corresponding to a totally disordered environment and 1 to perfect order. Even though there is some degree of local order in the LE phase, the crystalline order parameter $q^{(j)}$ very accurately discriminates lipids in the LC phase from lipids in the LE phase (except perhaps close or at the boundary between LC and LE domains). Also, it performs better than a criterion based on the number of neighbours (such as the Voronoi method) because $q^{(j)}$ is very sensitive to angular order of lipids in the neighbourhood of a given lipid.

In order to describe molecular orientation with respect to the monolayer we define the following unit vectors: (i) $\hat{\mathbf{n}}$, normal to the monolayer, which points along the $\pm z$ axes of the simulation box for the top and bottom monolayers, respectively; i.e. $\hat{\mathbf{n}}$ is defined at each of the water liquid-vapour interfaces as a normal vector pointing to the vapour side. (ii) $\hat{\mathbf{t}}$, the chain unit vector, which has been defined above. And (iii) $\hat{\mathbf{h}}$, the PN unit vector, defined to point from the phosphorous P atom to the nitrogen N atom of each lipid. We also define the projected components on the monolayer of these vectors as $\mathbf{t}_\perp = \hat{\mathbf{t}} - (\hat{\mathbf{t}} \cdot \hat{\mathbf{n}}) \hat{\mathbf{n}}$, $\mathbf{h}_\perp = \hat{\mathbf{h}} - (\hat{\mathbf{h}} \cdot \hat{\mathbf{n}}) \hat{\mathbf{n}}$, and their corresponding normalised versions $\hat{\mathbf{t}}_\perp$ and $\hat{\mathbf{h}}_\perp$.

With these vectors we define the distributions of the angles between the vector pairs $\{\hat{\mathbf{t}}, \hat{\mathbf{n}}\}$ (distribution of the tails about the monolayer normal), $\{\hat{\mathbf{h}}, \hat{\mathbf{n}}\}$ (distribution of the PN vector about the monolayer normal), and $\{\hat{\mathbf{t}}, \hat{\mathbf{h}}\}$ (distribution of the angle between tail and PN vectors). All of these distributions will be called *three-dimensional* (3D) distributions. In addition, we also compute the distribution of the angle between the vectors $\{\hat{\mathbf{t}}_\perp, \hat{\mathbf{h}}_\perp\}$.

This will be called *two-dimensional* (2D) distribution. Both 2D and 3D distributions will be computed separately for the LC and LE regions, using the method described above, to understand the different orientational properties of molecules in the two phases.

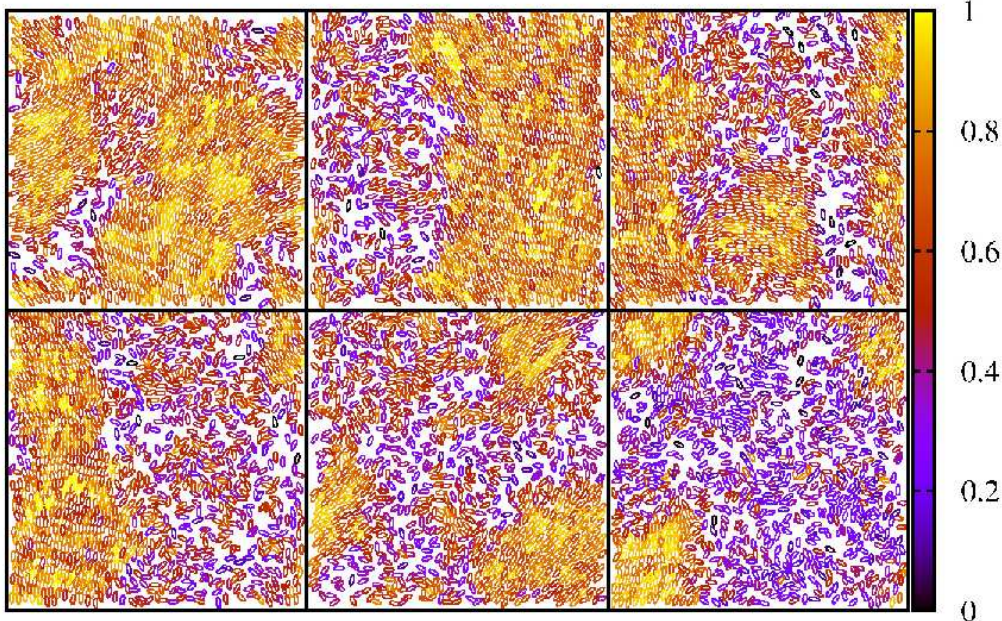


FIG. 3: Top configurations of one of the monolayers for different values of the mean area per lipid (from top-left panel and clockwise: 58 \AA^2 , 61 \AA^2 , 63 \AA^2 , 65 \AA^2 , 68 \AA^2 , and 71 \AA^2). Lipid molecules are represented as ellipses with an aspect ratio of 2, oriented along the projection of the tail vector on the monolayer. Ellipses are coloured according to the value of the crystalline order parameter $q^{(j)}$ (scale given by the accompanying colour bar).

III. RESULTS

A. Domain identification and domain shape

Fig. 3 shows top views of one of the two monolayers for typical configurations at different areas per lipid, ranging from the pure LC phase to the pure LE phase. Lipid chains are represented by ellipses of length-to-width ratio equal to 2, oriented along the projection of the tilt vector on the monolayer, and coloured according to the value of the crystalline order parameter at each lipid molecule. High values of $q^{(j)}$ are identified with the LC phase,

whereas low values correspond to LE regions. From this figure we see that, except in one case, the final separation stage of the phase transition has been reached, since only two coexisting domains of LC and LE regions exist in the monolayers. At high mean area per lipid LC domains are small, becoming bigger as the area per lipid is decreased. Domains are not circularly-shaped, as would be expected in systems with isotropic lateral interactions, but tend to be elongated when they are large enough. In other words, domain shapes seem to indicate that the curvature along the boundary is not constant. Also, there is a clear asymmetry between LC and LE domains as far as the sign of the curvature is concerned: While LC domains seem to have a preference for positive curvature, LE ones show negative curvatures. Crystallinity in LC domains appears to be quite uniform with only slight distortion of crystalline axes throughout the domains. Also note that a simple visual inspection of Fig. 3 seems to indicate that the projected tilt angle (i.e. the local crystalline axes) are at an oblique angle with respect to the interface, as it is also apparent in Fig. 2 of Javanainen et al.¹⁷.

Fig. 3 represents the projections of the molecules as ellipses of aspect ratio 2. The aspect ratio of a molecule on the monolayer plane is obtained by calculating the two-dimensional gyration tensor using the projected atomic coordinates. The ratio of the two eigenvalues of this tensor gives the aspect ratio $\kappa > 1$. Fig. 4 shows the distribution of κ in the LC and LE domains. As can be seen, both distributions have a maximum around $\kappa = 2$. The calculated mean aspect ratios in both regions are very close to 2.5.

B. Coexistence densities

Our ability to accurately identify domains and the molecules that belong to domains allows us to calculate the local two-dimensional density at the molecules separately in each phase. Local densities can be computed, regardless of the existence of domains, by counting the number of molecules within a circle of radius 0.7 nm centered at a given molecule. The resulting global distribution of local densities turns out to be unimodal since local densities in the LE regions vary by a large amount and, therefore, coexistence densities cannot be extracted directly from such a distribution. However, Javanainen et al.¹⁷ chose to determine the coexistence densities from a fit of the global distribution of local density, as obtained from a Voronoi tessellation, to two Gaussian functions, each representing the distribution of

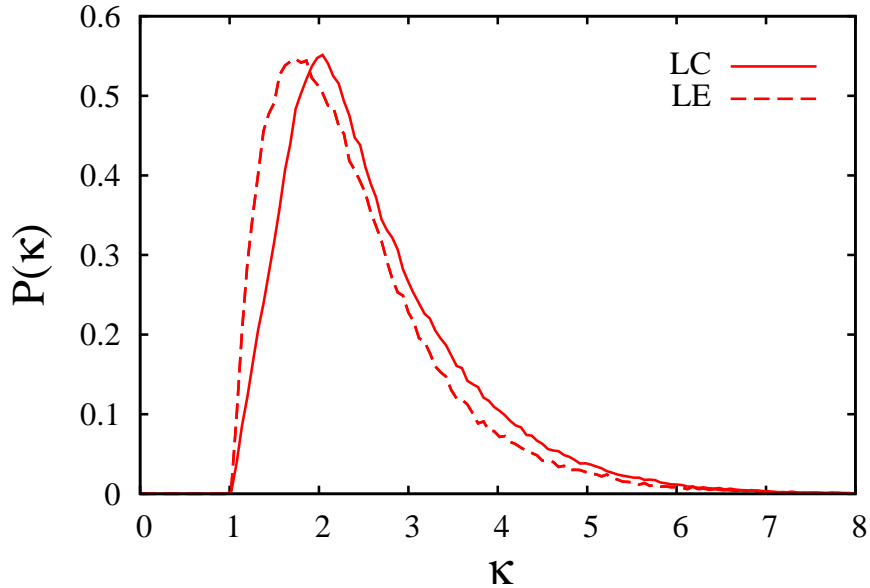


FIG. 4: Aspect-ratio distributions in the LC and LE domains for a mean area per lipid of 63 \AA^2 .

densities in one of the two coexisting phases. Instead, here we take advantage of our ability to identify domains to directly obtain the density distribution in each phase. Fig. 5 shows a histogram of the local areas per lipid for the two phases separately, for the cases where the mean area per lipid is 61 \AA^2 and 68 \AA^2 . The two distributions overlap, with the one corresponding to the LC domains being more localised (as expected for a phase with a high degree of crystallinity). However, their maxima are well separated and mean values can be obtained separately for each histogram. These values are 54.8 \AA^2 and 74.8 \AA^2 for a mean area per lipid of 61 \AA^2 , which coincide very well with the ones obtained from other values of mean areas per lipid. Note from the figure that the individual density distributions are not exactly Gaussians. This fact leads us to believe that our methodology could provide more reliable values for the coexistence densities.

C. 3D distributions

The spatial arrangement of the projected tail vectors shown in Fig. 3 confirms that lipid chains are oriented in the LC regions. This is of course a signature of the LC phase, which involves perfect side-to-side packing of aliphatic chains in planar, all-gauche conformations⁴.

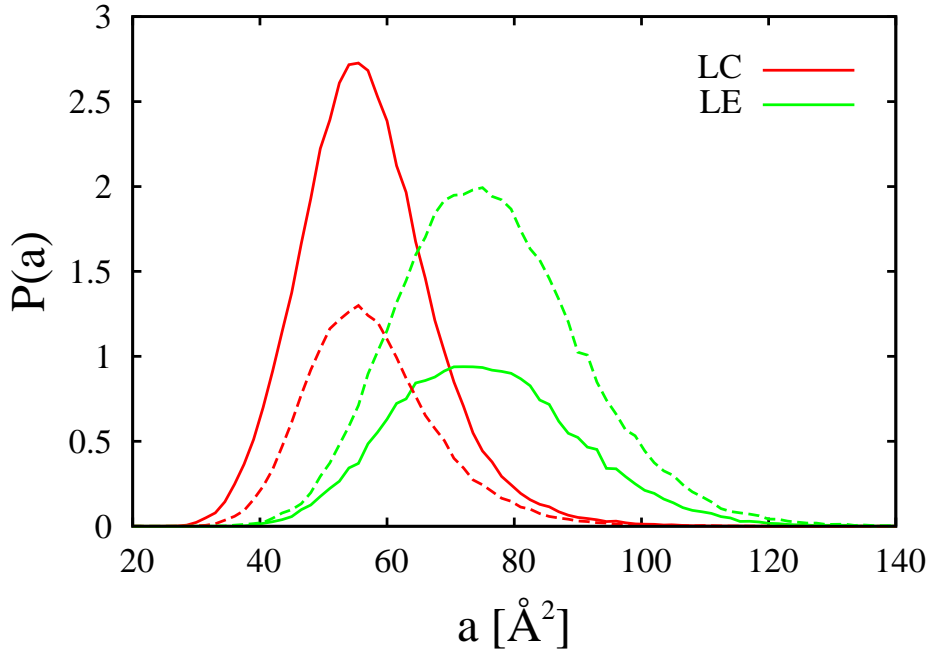


FIG. 5: Histograms of local areas per lipid for the LC and LE phases. Mean area per lipid is 61 \AA^2 (continuous curves) and 68 \AA^2 (dashed curves).

More important, visual inspection of the configurations points to global ordering of the tails in LC domains. Chains are not only ordered but also tilted with respect to the monolayer normal. The distributions in the chain angle are shown in Figs. 6 for LC (panel (a)) and LE (panel (b)) domains. These two distributions are largely independent of mean area per lipid, as expected since we are probing the coexistence region of a first-order phase transition. The distribution is strongly peaked in LC regions but much broader in LE regions, consistent with the model of straight and packed chains in the LC molecular configurations and disordered chains in the LE phase. From the mean of the distribution we obtain a tilt angle with respect to the outward interface normal of $(39.0 \pm 0.1)^\circ$ for the LC phase (standard deviation is obtained from the values for the different values of area per lipid). The value for the LE phase is $(48.1 \pm 0.5)^\circ$. This is less relevant as the distribution is much broader because of the high orientational disorder of chains.

The chain angle distribution has been measured previously by other authors using atomistic simulation. Choe et al.³¹ simulated a DPPC monolayer at higher temperature (325 K) and different mean area per lipid (56 \AA^2), in the supercritical region. Their distribution is

much more peaked than in our case, giving a mean tilt angle of $\sim 25^\circ$. This is not surprising, as we are probing the tilt angle at lower temperature and density. High density monolayers are known to exhibit a reduced tilt angle⁴. The same result for the chain angle was obtained by Domínguez et. al²³ for a similar temperature (323 K) but at a considerably lower density (mean area per lipid of 55 \AA^2). This seems to contradict the widely accepted idea that the tilt angle decreases as the monolayer is compressed. However, we should bear in mind that the two works use slightly different force fields, and also that the simulations use very small system sizes (90 and 32 lipid molecules, respectively).

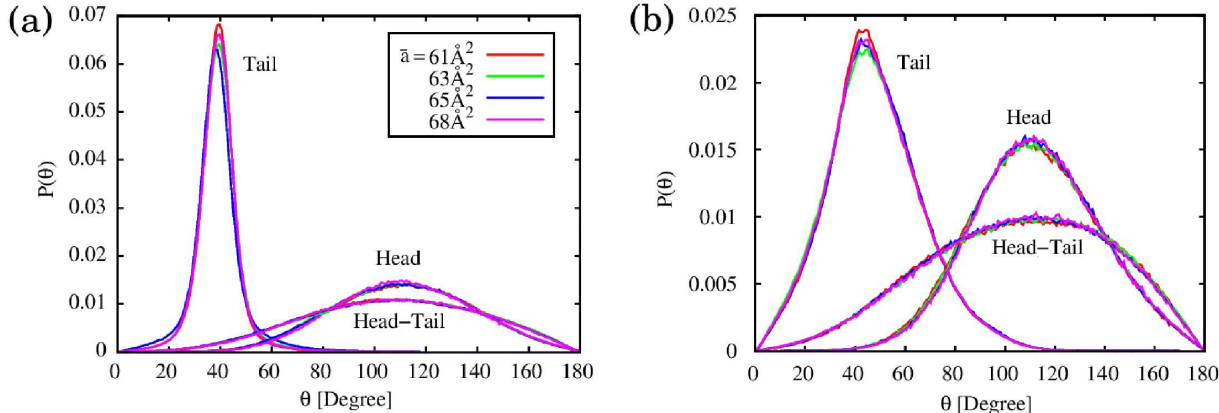


FIG. 6: (a) 3D distributions of chain angle, PN angle, and relative chain-PN angle in LC domains. (b) Same as in (a), but for LE domains. Mean areas per lipid \bar{a} are indicated in the key.

PN-dipole distributions are also plotted in Figs. 6(a) and (b) for the LC and LE domains. Again the dependence on mean area per lipid is weak. From the mean values we obtain tilt angles of $(110.8 \pm 0.5)^\circ$ for the LC phase and $(112.5 \pm 0.5)^\circ$ for the LE phase. Not only the tilt angle of the PN dipole is quite similar in the two phases, but also the full distributions. This implies that the phase transition mainly involves a configurational change of the lipid chains and that the distribution of dipoles does not significantly depend on the local lipid density. This conclusion is consistent with the experimental studies of Hauser et al.³² and of Ma and Allen¹³. On the other hand, Mohammad-Aghaie et al.¹⁵ report a bimodal PN-dipole distribution in the LC phase for a slightly lower temperature, using the GROMOS force field and a monolayer of 64 lipid molecules. The bimodality tends to disappear as temperature increases. Sun³³ reports a simulation of a monolayer with 56 molecules of a lipid similar to DPPC (same polar head but longer tail), using the CHARMM27 force field

at a temperature of 293 K. The PN-dipole distribution also turns out to be bimodal. This feature is attributed³³ to two competing dipole orientations. However, the origin of the two favoured orientations is not clear. Our distributions, by contrast, show no signature of bimodality, as would correspond to a truly equilibrated LC phase that coexist with a LE phase. Since domains of coexisting LE and LC phases are clearly identified in our simulation and system size is much larger than in previous works^{15,33}, signatures of both phases are not mixed in our simulation, and lack of relaxation to equilibrium is probably not an issue. Also note that our results indicate that the PN-dipole distributions in the LC and LE phases are almost identical, as can be inferred from Figs. 6(a) and (b) by comparing their heights and taking into account that both distributions are normalized.

Another very interesting distribution involves the angle between chains and head dipoles, also shown in the figures. The results are rather surprising, since they imply very broad distributions, even in the LC phase. Their means, $(71.8 \pm 0.6)^\circ$ and $(75.5 \pm 0.5)^\circ$ for LC and LE phases, respectively, are consistent with the mean values for the chain and PN-dipole distributions, but the fact that the distributions are so broad implies a high degree of rotational freedom in the azimuthal angle for the PN dipole in both phases.

D. 2D distributions

To confirm the scenario that results from the 3D distributions, we have also calculated the corresponding distributions of the projected chain and PN-dipole vectors, and of their relative angle. Even though the projected chains show a high degree of angular order extending throughout LC domains, see Fig. 3, their distribution is considerably blurred when referred to a fixed direction in the monolayer because of the deformations of the vector fields within the domains. The PN-dipole distribution suffers from the same problem. Therefore we only show the distribution in the relative angle between the projected chain and PN-dipole vectors in Fig. 7 for the LC and LE domains, averaged over the whole coexistence region. Here we clearly see that the PN-dipole projection is almost completely disordered with respect to the well defined local chain orientation, confirming the conclusion drawn from the 3D distributions that PN dipoles exhibit almost full rotational libration in the azimuthal angle.

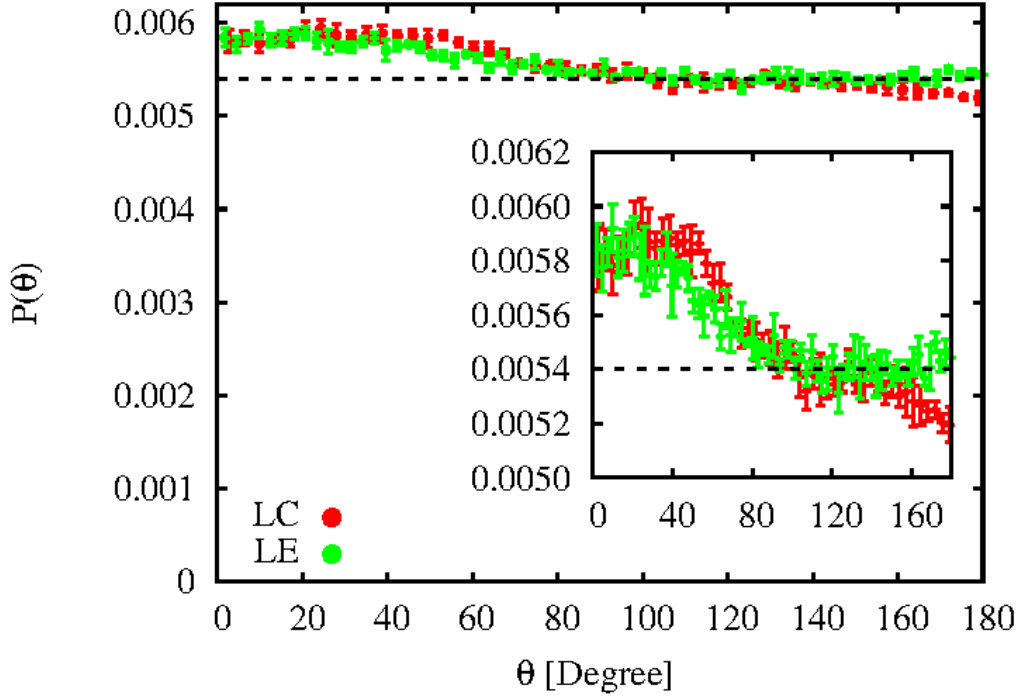


FIG. 7: Angle between projected head and tail in LC and LE domains.

E. Correlation functions

The above results, inferred from angular 2D and 3D distributions, are confirmed by calculating different correlation functions. We define $f_k^{(t)}(r) \equiv \langle \cos k\varphi \rangle(r)$ as a radial correlation function, where $\cos \varphi = \hat{\mathbf{t}}_{\perp}(\mathbf{0}) \cdot \hat{\mathbf{t}}_{\perp}(\mathbf{r}_{\perp})$, $\hat{\mathbf{t}}_{\perp}(\mathbf{0})$ is the projected unit tail vector for a molecule located at the origin, and $\hat{\mathbf{t}}_{\perp}(\mathbf{r}_{\perp})$ is the same vector but for a molecule at a transverse distance from the latter given by the vector \mathbf{r}_{\perp} . The angular brackets $\langle \dots \rangle$ mean average over molecules and time. Therefore, $f_1^{(t)}(r)$ and $f_2^{(t)}(r)$ measure angular correlations in the monolayer. Similar functions $f_1^{(m)}(r)$ and $f_2^{(m)}(r)$ can be defined and computed for the projected PN vectors. Extracting all these four functions separately for the two types of domains is simple, as molecules can be identified as belonging to one phase or the other. However, due to the finite size of the domains, the long- and intermediate-range behaviour of the functions have to be interpreted with care.

Figs. 8 shows these functions for LC and LE regions and for several values of mean area per lipid. We can see, panels (a) and (c), that long-range correlations are quite evident in both polar and nematic correlations for the tails in the LC domains, as expected from the

high degree of orientation in LC domains. The functions exhibit weak oscillations at short distances and stronger quasi-long range order at long distances as domains become larger. By contrast, correlations between PN heads rapidly decay with distance, panels (b) and (d). These panels compare the corresponding functions for tails and heads, and show the dramatically different behaviours. These results are consistent with the conclusions drawn from the angular distributions. While one would expect the packed hydrocarbon chains to give rise to strong correlations at long distances in the LC phase, and water-solvated head groups to exhibit damped behaviour, the absence of correlations in the latter is somewhat surprising.

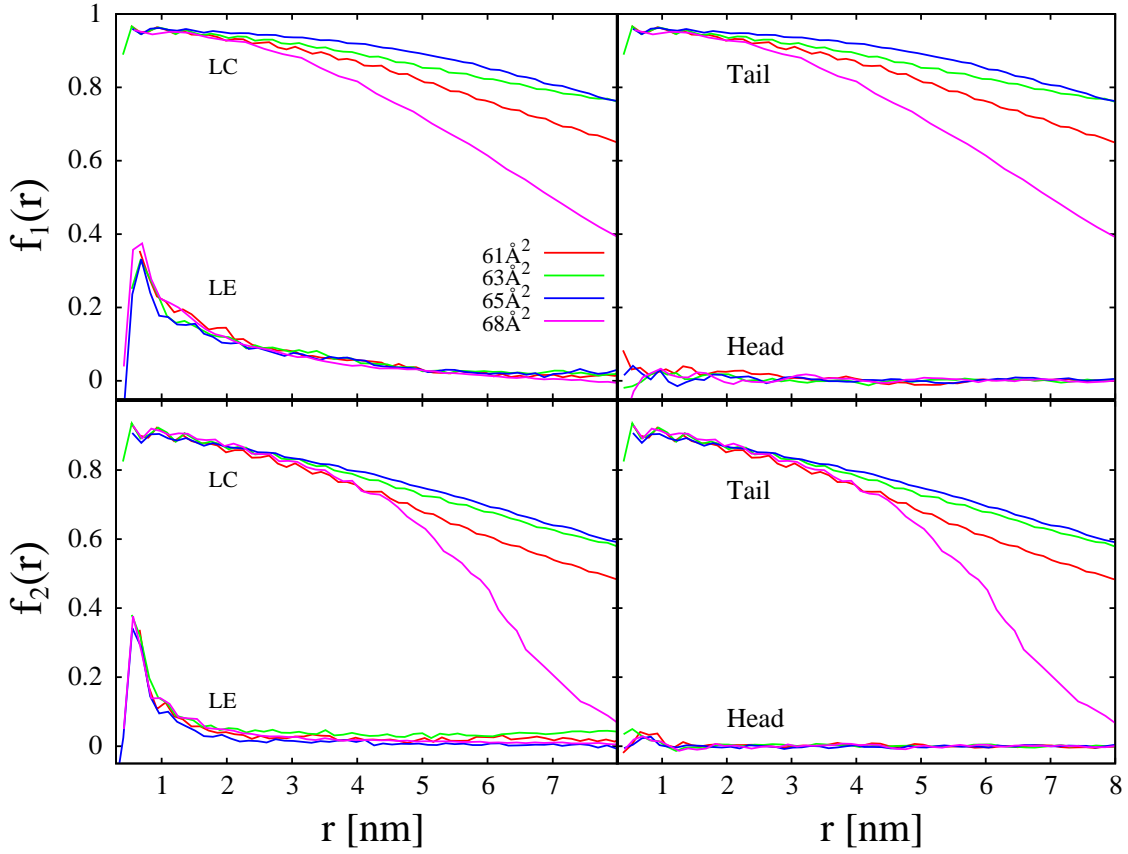


FIG. 8: Correlation functions $f_1(r)$ and $f_2(r)$. (a) and (c): tail correlation functions $f_1^{(t)}(r)$ and $f_2^{(t)}(r)$ for different mean areas per lipid and for the two regions LE and LC. (b): $f_1^{(t)}(r)$ and $f_1^{(m)}(r)$ for the LC domains. (d) $f_2^{(t)}(r)$ and $f_2^{(m)}(r)$ for the LC domains. In all cases mean areas per lipid are given by the key in (a).

F. Penetration of lipid molecules into the subphase in LE and LC domains

Several authors (see Ref.²⁵ and references therein) have speculated on the different arrangement of lipid molecules in the LC and LE phases. In particular, it is believed that the PN dipole is located deeply into the aqueous subphase in the LE regions and that, as chains become closely packed because of the increased lateral pressure, solvation water around dipoles is expelled which forces the dipoles to become closer to the water surface. In order to investigate this, we have calculated the density profiles across the interface for the water and lipid molecules in both phases. These are shown in Fig. 9, where the densities refer to the whole mass content of lipid and water molecules separately, including all interaction centres in both cases. The horizontal axis is the z coordinate in the frame attached to the simulation box. The profiles correspond to a mean area per lipid of 63 \AA^2 , where approximately 50% of each monolayer consists of a single LC domain. Density profiles are presently separately for the two regions, LC and LE. Therefore, the density profile for water corresponds to the water column below the corresponding domain. Since domains are large, we expect small interface fluctuations in both LC and LE regions; the fact that the density profiles of water have the same shape implies that the rigidity of the interface is similar in both cases. It can be seen that the lipid distribution in the LC domains develops a shoulder and becomes wider. This is due to the crystallisation of the molecular chains. But two features of the profiles are particularly interesting: (i) the water profiles are very similar in both phases, except for a shift in their position; (ii) the penetration of the molecular polar heads in water is the same in both regions. The latter feature is more apparent if the LC profiles are rigidly displaced to make both water profiles coincide (see inset): the polar heads show no relative change with respect to water. Our conclusions are that, on the one hand, the polar heads do not approach the water interface as LC domains are formed at the LE-LC phase transition and, as a consequence, the hydration state of the polar head is not changed. And, on the other hand, the water interface appears to be displaced by polar heads as they reorganise as a result of molecular chains becoming more closely packed in LC domains.

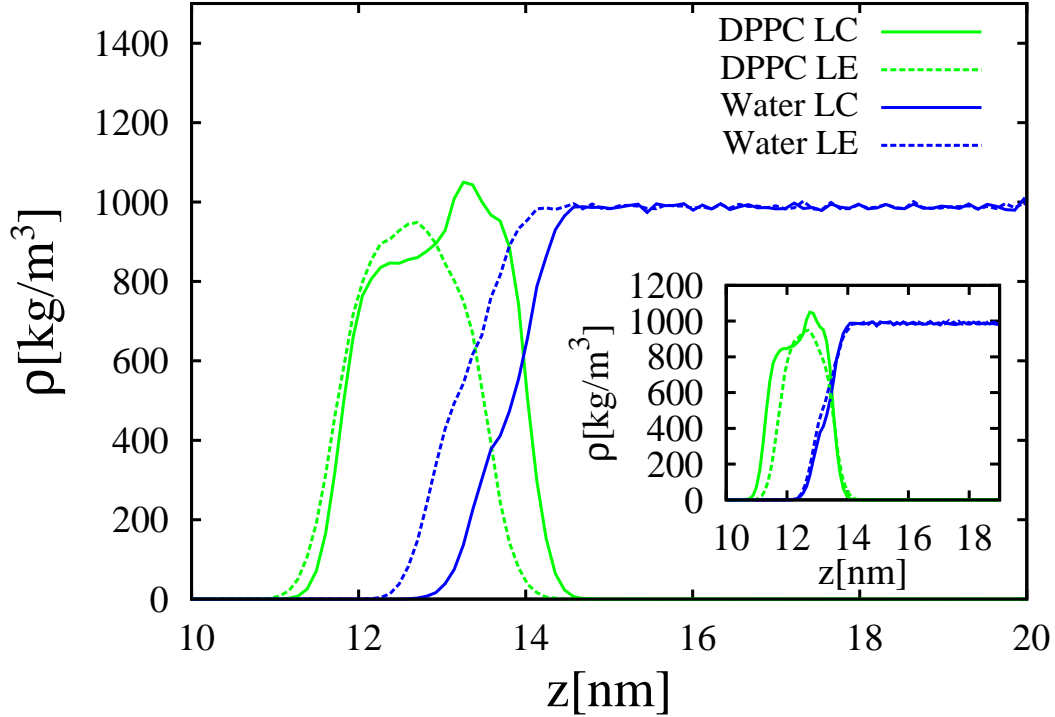


FIG. 9: Mass density profiles of lipid and water molecules corresponding to one of the monolayers at a mean area per lipid of 63 \AA^2 , for both LC and LE regions. In the inset the LC profiles have been displaced so as to make the water profiles in both regions coincide.

IV. CONCLUSIONS

In this work we have analyzed the coexistence region between LC and LE phases in a DPPC monolayer. For the first time, the properties of the coexisting phases have been studied separately by identifying the molecules that belong to each phase. Moreover, the present simulations involve considerably larger system sizes than previous works. In practice, simulation times have been long enough to allow the system to phase separate completely which ensures that true equilibrium states of the monolayer are being analyzed. By contrast, previous works so far have focused on the properties of phases without imposing coexistence conditions. This strategy does not avoid the presence of domains of the opposite phase which might contaminate the averaged properties of the phase under consideration.

Several conclusions from the present simulation study confirm previous results from other groups. For example, the angular distribution of the tilt angle of chains is consistent with the

ones reported previously^{23,31}. Visual inspection of the projected molecular shows that there is a high degree of order in LC domains while the distribution is uniform in LE domains.

As for the PN-dipole distributions, we conclude that tilt angle distribution is always unimodal and very similar in both phases. The average angle is about 111° , i.e. the PN dipole points 21° towards the water from the monolayer plane. This value is much larger than the previously reported value of $\sim 5^\circ$, and implies a much larger contribution to the molecular dipole perpendicular to the monolayer. Comparison of this result with previous studies is hindered by the very different thermodynamic states used in those works. In particular, Mohammad-Aghaie et al.¹⁵ report a bimodal distribution for a supposedly pure LC phase. Such a bimodal distribution is difficult to understand for a pure phase in equilibrium.

In addition, we have also explored the distribution of the angle between the projected chain and PN-dipole vectors. To our knowledge this is the first time such an azimuthal distribution is reported. Assuming a some degree of rigidity in the molecular structure of the lipid molecules, we would expect a high correlation between the orientation of the chains and of the PN head in a monolayer of DPPC molecules. However, at least within the present force fields, this does not seem to be the case. According to our results, the polar angle of PN heads has a well defined value, but the head seems to be subject to almost free librations in the azimuthal angle (angle measured in the plane of the monolayer). Further work on this point may require a more detailed investigation of the reliability of the present force field and more structural results from the experimental side. The present results indicate that the component of the dipolar moment parallel to the monolayer, which is larger than the perpendicular component, would play no role since it is completely disordered, even in LC domains. This is in contrast with common wisdom according to which the PN dipole adopts a close-to-parallel configuration in the LC phase, whereas in the LE phase it has a more flexible orientation that can change with respect to the packed LC configuration.

Contrary to earlier suggestions²⁵, our results indicate that lipid molecules show the same degree of penetration in the water side of the interface, regardless of the phase, LE or LC. Instead, strong vdW forces between chains appear to give rise to a displacement of the whole interface. However, this feature might be a consequence of the force fields used and the treatment of the head-group hydration, which depends sensitively on force field and molecular geometry.

LC domains are observed to be elongated, as discussed by many authors⁸⁻¹¹. Their shape

is not elliptical but rather resembles a discorectangle. However longer simulations would be necessary to confirm this issue. Nonspherical shapes may be induced by competition between various relevant forces, more importantly vdW forces showing up as a line tension, and forces from perpendicular dipoles. The strong alignment of lipid chains along domain boundaries may imply the presence of a significant anisotropic line tension, which should be incorporated to the theoretical models^{34,35}. Also, visual inspection of the domains shows that the sign of the curvature may be an important ingredient in theoretical models.

Acknowledgments

We acknowledge financial support from grants FIS2017-86007-C3-1-P and FIS2017-86007-C3-2-P from Ministerio de Economía, Industria y Competitividad (MINECO) of Spain. Work in DPTs groups is supported by the Natural Sciences and Engineering Research Council (Canada), with additional support from the Canada Research Chair Program. Simulations were carried out on Compute Canada resources, funded by the Canada Foundation for Innovation and partners. SP wishes to acknowledge financial support from MINECO through a FPI PhD fellowship.

S. Panzuela ORCID: 0000-0002-0177-7888

D. P. Tieleman ORCID: 0000-0001-5507-0688

L. Mederos ORCID: 0000-0002-4579-8680

E. Velasco ORCID: 0000-0002-7350-1813

* Electronic address: sergio.panzuela@uam.es

† Electronic address: tieleman@ucalgary.ca

‡ Electronic address: lmederos@icmm.csic.es

§ Electronic address: enrique.velasco@uam.es

¹ Wütnecka, R.; Pérez-Gil, J.; Wüstnecka, N.; Cruzbi, A.; Fainermaan V. B.; Pison, U. Interfacial Properties of Pulmonary Surfactant Layers. *Adv. Colloid Interface Sci.* **2005**, 117, 33-58.

² Parra, E.; Pérez-Gil, J. Composition, structure and mechanical properties define performance of pulmonary surfactant membranes and films. *Chem. Phys. Lipids* **2008**, 185, 153-175.

- ³ Casals, C; Cañadas, O. Role of lipid ordered/disordered phase coexistence in pulmonary surfactant function. *Biochim. Biophys. Acta* **2012**, 1818, 2550-2562.
- ⁴ Kaganer, V. M.; Möhwald, H.; Dutta, P. Structure and Phase Transitions in Langmuir Monolayers. *Rev. Mod. Phys.* **1999**, 71, 778-891.
- ⁵ Baoukina, S.; Tieleman, D. P. Computer simulations of lung surfactant. *Biochim. Biophys. Acta-Biomembranes* **2016**, 1858, 2431-2440.
- ⁶ Baoukina, S.; Mendez-Villuendas, E.; Tieleman, D. P. Molecular view of phase coexistence in lipid monolayers. *JACS* **2012**, 134, 17543-17553.
- ⁷ Duncan, S. L.; Larson, R. G. Comparing Experimental and Simulated Pressure-Area Isotherms for DPPC. *Biophys. J.* **2008**, 94, 2965-2986.
- ⁸ Moy, V. T.; Keller, D. J.; Gaub, H. E.; McConnell, H. M. Long-Range Molecular Orientational Order in Monolayer Solid Domains of Phospholipid. *J. Phys. Chem.* **1986**, 90, 3198-3202.
- ⁹ Keller, D. J.; Korb, J. P.; McConnell, H. M. Theory of Shape Transitions in Two-Dimensional Phospholipid Domains. *J. Phys. Chem.* **1987**, 91, 6417-6422.
- ¹⁰ McConlogue, C. W.; Vanderlick, T. K. A Close Look at Domain Formation in DPPC Monolayers. *J. Phys. Chem.* **1987**, 91, 6417-6422.
- ¹¹ Flörsheimer, M.; Möhwald, H. Development of Equilibrium Domain Shapes in Phospholipid Monolayers. *Chemistry and Physics of Lipids* **1989**, 49, 231-241.
- ¹² Möhwald, H. Phospholipid and Phospholipid-Protein Monolayers at the Air/Water Interface. *Annu. Rev. Phys. Chem.* **1990**, 41, 441-476.
- ¹³ Ma, G.; Allen, H. C. DPPC Langmuir Monolayer at the Air-Water Interface: Probing the Tail and Head Groups by Vibrational Sum Frequency Generation Spectroscopy. *Langmuir* **2006**, 22, 5341-5349.
- ¹⁴ Rose, D.; Rendell, J.; Lee, D.; Nag, K.; Booth, V. Molecular Dynamics Simulations of Lung Surfactant Lipid Monolayers. *Biophys. Chem.* **2008**, 138, 67-77.
- ¹⁵ Mohammad-Aghaie, D.; Macé, E.; Sennoga, C. A.; Seddon, J. M.; Bresme, F. Molecular Dynamics Simulations of Liquid-Condensed to Liquid-Expanded Transitions in DPPC Monolayers. *J. Phys. Chem. B* **2010**, 114, 1325-1335.
- ¹⁶ Huynh, L; Perrot, N.; Beswick, V.; Rosilio, V.; Curmi, P. A.; Sanson, A.; Jamin, N. Structural Properties of POPC Monolayers under Lateral Compression: Computer Simulation Analysis. *Langmuir* **2014** 30, 564-573.

- ¹⁷ Javanainen, M.; Lamberg, A.; Cwiklik, L.; Vattulainen, I.; Samuli Ollila, O. H. Atomistic Model for Nearly Quantitative Simulations of Langmuir Monolayers. *Langmuir* **2018**, *34*, 2565-2572.
- ¹⁸ Klauda, J. B.; Venable, R. M.; Freites, J. A.; O'Connor, J. W.; Tobias, D. J.; Mondragon-Ramirez, C.; Vorobyov, I.; Mackerell, A. D., Jr; Pastor, R. W. Update of the CHARMM All-Atom Additive Force Field for Lipids: Validation on Six Lipid Types. *J. Phys. Chem. B.* **2010**, *114*, 7830-7843.
- ¹⁹ Izadi, S.; Anandakrishnan, R.; Onufriev, A. V. Building Water Models: A different Approach. *J. Phys. Chem. Lett.* **2014**, *5*, 3863-3871.
- ²⁰ Pronk, S.; Páll, S.; Schulz, R.; Larsson, P.; Bjelkmar, P.; Apostolov, R.; Shirts, M. R.; Smith, J. C.; Kasson, P. M.; van der Spoel, D.; Hess, B.; Lindahl, E. GROMACS 4.5: A High-Throughput and Highly Parallel Open Source Molecular Simulation Toolkit. *Bioinformatics* **2013**, *29*, 845-854.
- ²¹ Abraham, M. J.; Murtola, T.; Schulz, R.; Páll, S.; Smith, J. C.; Hess, B.; Lindahl, E. GROMACS: High Performance Molecular Simulations Through Multi-Level Parallelism From Laptops to Supercomputers. *SoftwareX* **2015**, 1-2, 19-25.
- ²² in 't Veld, P. J.; Ismail, A. E.; Grest, G. S. Application of Ewald Summations to Long-Range Dispersion Forces. *J. Chem. Phys.* **2007**, *127*, 144711.
- ²³ Dominguez, H.; Smondyrev, A. M.; Berkowitz, M.L. Computer Simulations of Phosphatidylcholine Monolayers at Air/Water and CCl₄/Water Interfaces. *J. Phys. Chem. B* **1999**, *103*, 9582-9588.
- ²⁴ Hauser, H.; Phillips, M. C. in: Danielli, J. F.; Rosenberg, M.D.; Cadenhead, D. A. (Eds.), *Progress in Surface and Membrane Science* **1979**, *13*, 297 (Academic Press, New York).
- ²⁵ Miñones Jr, J.; Rodríguez Patino, J. M.; Conde, O.; Carrera, C.; Seoane, R. The Effect of Polar Groups on Structural Characteristics of Phospholipid Monolayers Spread at the Air-Water Interface. *Col. Surf. Sci. A: Physicochem. Eng. Aspects* **2002**, *203*, 273-286.
- ²⁶ Sriram, I.; Schwartz, D. K. Line tension between coexisting phases in monolayers and bilayers of amphiphilic molecules. *Surf. Sci. Rep.* **2012**, *6*, 143-159.
- ²⁷ Lamberg, A.; Samuli Ollila, O. H. Comment on 'Structural Properties of POPC Monolayers under Lateral Compression: Computer Simulation Analysis'. *Langmuir* **2015**, *31*, 886-887.
- ²⁸ Huynh, L.; Perrot, N.; Beswick, V.; Rosilio, V.; Curmi, P. A.; Sanson, A.; Jamin, N. Reply to 'Comment on "Structural Properties of POPC Monolayers under Lateral Compression: Com-

- puter Simulation Analysis". *Langmuir* **2015**, 31, 888-889.
- ²⁹ Mohammad-Aghaie, D.; Bresme, F. Force-field Dependence on the Liquid-Expanded to Liquid-Condensed Transition in DPPC Monolayers. *Mol. Simul.* **2016**, 42, 391-397.
- ³⁰ Baoukina, S.; Monticelli, L.; Marrink, S. J.; Tieleman, D. P. Pressure-Area Isotherm of a Lipid Monolayer from Molecular Dynamics Simulations. *Langmuir* **2007**, 23, 12617-12623.
- ³¹ Choe, S.; Chang, R.; Jeon, J.; Violi, A. Molecular Dynamics Study of a Pulmonary Surfactant Film interacting with a Carbonaceous Nanoparticle. *Biophys. J.* **2008**, 95, 4102-4114.
- ³² Hauser, H.; Pascher, I.; Pearson, R.; Sundell, S. Preferred Conformation and Molecular Packing of Phosphatidylethanolamine and Phosphatidylcholine. *Biochim. Biophys. Acta* **1981**, 650, 21-51.
- ³³ Sun, F. Constant Normal Pressure, Constant Surface Tension, and Constant Temperature Molecular Dynamics Simulations of Hydrated 1,2-Dilignoceroylphosphatidylcholine Monolayer. *Biophys. J.* **2002**, 82, 2511-2519.
- ³⁴ McConnell, H. M.; Moy, V. T. Shapes of finite two-dimensional lipid domains. *J. Phys. Chem.* **1988**, 92, 4520-4525.
- ³⁵ Campelo, F; Cruz, A.; Pérez-Gil, J.; Vázquez, L.; Hernández-Machado, A. Phase-field Model for the Morphology of Monolayer Lipid Domains. *Eur. Phys. J. E* **2012**, 35, 49.